# A Quadratic Assumed Natural Strain Curved Triangular Shell Element

**K.Y.Sze** and **Dan Zhu***

*Department of Mechanical Engineering, The University of Hong Kong*

*Pokfulam Road, HONG KONG*

**ABSTRACT**

In this paper, a six-node triangular $C^0$ curved shell element is developed by the assumed natural or covariant strain (ANS) method. While the element is quadratic in nature, the sampled natural strains are optimal with respect to the derivative of a prescribed cubic field in a subparametric element. Numerical examinations reveal that the element shows no sign of locking, passes all the patch tests and yields satisfactory accuracy.

* on leave from Southwest Jiaotong University, Chengdu, Sichuan 610031, P.R.CHINA

Published in *Computer Methods Appl.Mech.Engrg.* 174 (1999) 57-71

## 1. INTRODUCTION

Automatic meshing and adaptive mesh refinement are becoming standard features of the state-of-the-art finite element software. It is note worthy that triangular mesh is often the preferred choice of most mesh generators. Consequently, the improvement of triangular elements should be envisaged. In this paper, a quadratic triangular curved shell element is developed with the following criteria in mind : (a) its kinematic has not been modified by the Kirchhoff or zero transverse shear constraints so that it is applicable to thick and composite/sandwich plates/shells; (b) it does not possess any commutable mechanism; (c) its boundary nodes have the same number of d.o.f.s so that it presents no complication for being implemented in any finite element code; (d) it passes constant moment and constant transverse shear patch tests under the flat plate geometry; (e) it does not exhibit shear locking; (f) it passes the constant membrane stress patch test under the flat plate geometry and (g) it does not exhibit membrane locking.

Our literature survey indicated that T6/3-B3 *(displacement model with six boundary nodes and three bubble heterosis nodes)* [1], MITC7 *(assumed strain model with six boundary nodes and one bubble heterosis node)* [2], TRI-6 *(assumed strain model with six boundary nodes only)* [3], T6/3* *(displacement model with six boundary nodes only)* [4,5], AST6 *(assumed strain model with six boundary nodes only)* [4], ANS6P *(assumed natural strain model with only six boundary nodes)* [6] are probably the only quadratic plate bending elements that satisfy criteria (a) to (e). While T6/3-B3 and TRI-6 appear to be too flexible, MITC7 is at least twice more expensive than TRI-6. T6/3* is the same as the conventional six-node displacement model except that it is integrated by a less popular three-point rule whose sampling points coincide with the mid-side nodes. Though T6/3* does not exhibit shear locking, it is poor in accuracy. Assumed strain element AST6 and assumed natural strain element ANS6P have been developed very recently by the authors and their coworker. They are as economic as TRI-6 but competitive to MITC7 in accuracy.

Regarding the quadratic $C^0$ shells, the popular COMPENDEX CD-ROM database for engineering publications have been searched from the year 1986 to 1996 with the following conjunctive selection criteria : subject “finite element method”, title words “shell” and “triangular”. Out of the twenty-six identified articles, only four of them are on curved shell elements [7-10] whereas the others are on facet shells. The shell counterparts of T6/3-B3, MITC7 and TRI-6 are not found. The degenerated element presented in reference [7] does not contains rotations as d.o.f.s. It involves rather complicated theory of differential geometry and no information is given whether the element is immune from membrane locking. Moreover, none of the models presented in references [8-10] meets our criteria.

In this paper, a $C^0$ six-node curved triangular shell element that fulfilling all our criteria are developed by generalizing our previously devised ANS6P plate bending element [6].

## 2. GEOMETRY AND KINEMATIC FOR SIX-NODE $C^0$ SHELL ELEMENT

This section describes the geometry and kinematic of the conventional or purely displacement-based six-node shell based on the degenerated solid approach [11-13].

*2.1 Global Cartesian Coordinates and Natural Coordinates* Fig.1 shows a six-node curved shell element. Global Cartesian coordinates ($X$,$Y$,$Z$) of any point along the $i$-th nodal normal can be expressed as :

$$\mathbf{X}_i = \mathbf{X}_{oi} + \zeta \mathbf{X}_{ni} \tag{1a}$$

where $\zeta \in [-1,+1]$ is the transverse natural coordinate, $\mathbf{X}_{oi}$ is the position vector of the node and $\mathbf{X}_{ni}$ is the nodal normal vector. It can be noted that $\|\mathbf{X}_{ni}\|$, the magnitude of $\mathbf{X}_{ni}$, equals half of the nodal thickness $h_i$. The mapping between the global Cartesian coordinates ($X$,$Y$,$Z$) and the parametric coordinates ($s$,$t$,$\zeta$), where $s$ and $t \in [0,1]$ are the area coordinates, is set up by the standard interpolation :

$$\mathbf{X}(s,t,\zeta) = \sum_{i=1}^{6} N_i(s,t)\mathbf{X}_i = \mathbf{X}_o(s,t) + \zeta \mathbf{X}_n(s,t) \tag{1b}$$

where

$$\mathbf{X}_o = \sum_{i=1}^{6} N_i(s,t)\mathbf{X}_{oi} \ , \ \mathbf{X}_n = \sum_{i=1}^{6} N_i(s,t)\mathbf{X}_{ni}$$

$$N_1 = (1\text{-}s\text{-}t)(1\text{-}2s\text{-}2t) \ , \ N_2 = s(2s\text{-}1) \ , \ N_3 = t(2t\text{-}1) \ , \ N_4 = 4st \ , \ N_5 = 4t(1\text{-}s\text{-}t) \ , \ N_6 = 4s(1\text{-}s\text{-}t)$$

It is apparent that the mid-surface of the shell is given by the interpolated $\mathbf{X}_o$.

*2.2 Description of Element Kinematics* At each node, two vectors both of magnitude equal to half of the nodal thickness are defined as following :

$$\mathbf{f}_i^1 = \begin{cases} \dfrac{h_i}{2}\dfrac{\mathbf{X}_{ni} \times \mathbf{e}_Z}{\|\mathbf{X}_{ni} \times \mathbf{e}_Z\|} = \dfrac{h_i}{2}\dfrac{[Y_{ni}, -X_{ni}, 0]^T}{\sqrt{X_{ni}^2 + Y_{ni}^2}} & \text{for} \quad X_{ni}^2 + Y_{ni}^2 \neq 0 \\ \dfrac{h_i}{2}[1,0,0]^T & \text{for} \quad X_{ni}^2 + Y_{ni}^2 = 0 \end{cases} \tag{2a}$$

and

$$\mathbf{f}_i^2 = \frac{2}{h_i}(\mathbf{X}_{ni} \times \mathbf{f}_i^1) \tag{2b}$$

where $\mathbf{e}_Z = [0,0,1]^T$ is the unit vector in the Z-direction. Besides the three nodal translations $U_{oi}$, $V_{oi}$ and $W_{oi}$, two nodal rotations $\theta_i^1$ and $\theta_i^2$ which are the rotations about $\mathbf{f}_i^1$ and $\mathbf{f}_i^2$ are employed as the kinematic d.o.f.s, see Fig.1. Thus, the displacement at any point along the i-th nodal normal is :

$$\mathbf{U}_i = \mathbf{U}_{oi} + \zeta \mathbf{U}_{ni} \tag{3a}$$

in which

$$\mathbf{U}_i = \begin{bmatrix} U_i & V_i & W_i \end{bmatrix}^T \ , \ \mathbf{U}_{oi} = \begin{bmatrix} U_{oi} & V_{oi} & W_{oi} \end{bmatrix}^T \ , \ \mathbf{U}_{ni} = \begin{bmatrix} -\mathbf{f}_i^2 & \mathbf{f}_i^1 \end{bmatrix} \begin{Bmatrix} \theta_i^1 \\ \theta_i^2 \end{Bmatrix}$$

Similar to the coordinates, the interpolated displacement is :

$$\mathbf{U}(s,t,\zeta) = \sum_{i=1}^{6} N_i(s,t)\mathbf{U}_i = \mathbf{U}_o(s,t) + \zeta \mathbf{U}_n(s,t) \tag{3b}$$

where

$$\mathbf{U}_o = \mathbf{U}_o(s,t) = \sum_{i=1}^{6} N_i(s,t)\mathbf{U}_{oi} = \begin{bmatrix} N_1\mathbf{I}_3, \mathbf{0}_{3\times 2}, \ldots, N_6\mathbf{I}_3, \mathbf{0}_{3\times 2} \end{bmatrix} \mathbf{q}$$

$$\mathbf{U}_n = \mathbf{U}_n(s,t) = \sum_{i=1}^{6} N_i(s,t)\mathbf{U}_{ni} = [\mathbf{0}_{3\times 3}, -\mathbf{f}_1^2 N_1, \mathbf{f}_1^1 N_1, \ldots, \mathbf{0}_{3\times 3}, -\mathbf{f}_6^2 N_6, \mathbf{f}_6^1 N_6]\mathbf{q}$$

$\mathbf{q} = [U_1, V_1, W_1, \theta_1^1, \theta_1^2, \ldots, U_6, V_6, W_6, \theta_6^1, \theta_6^2]^T$ is the element displacement vector

*2.3 Covariant Strains* The inplane and transverse shear covariant strains defined with respect to the *s*-*t*-ζ-coordinates are [12-14] :

$$\varepsilon_{ss} = \mathbf{X}_{,s}^T \mathbf{U}_{,s} \ , \ \varepsilon_{tt} = \mathbf{X}_{,t}^T \mathbf{U}_{,t} \ , \ 2\varepsilon_{st} = \mathbf{X}_{,s}^T \mathbf{U}_{,t} + \mathbf{X}_{,t}^T \mathbf{U}_{,s} \tag{4a}$$

$$\gamma_{\zeta s} = \mathbf{X}_{,\zeta}^T \mathbf{U}_{,s} + \mathbf{X}_{,s}^T \mathbf{U}_{,\zeta} \ , \ \gamma_{\zeta t} = \mathbf{X}_{,\zeta}^T \mathbf{U}_{,t} + \mathbf{X}_{,t}^T \mathbf{U}_{,\zeta} \tag{4b}$$

By retaining up to the first order ζ-terms in the inplane strains ($\varepsilon_{ss}$ , $\varepsilon_{tt}$ and $2\varepsilon_{st}$) and the zeroth order ζ-terms in the transverse shear strains ($\gamma_{\zeta s}$ and $\gamma_{\zeta t}$), we have

$$\varepsilon_{ss} = \varepsilon_{ss}^m + \zeta\varepsilon_{ss}^b \ , \ \varepsilon_{tt} = \varepsilon_{tt}^m + \zeta\varepsilon_{tt}^b \ , \ 2\varepsilon_{st} = 2\varepsilon_{st}^m + 2\zeta\varepsilon_{st}^b \tag{5a}$$

where

$$\varepsilon_{ss}^m = \mathbf{X}_{o,s}^T\mathbf{U}_{o,s} \ , \ \varepsilon_{tt}^m = \mathbf{X}_{o,t}^T\mathbf{U}_{o,t} \ , \ 2\varepsilon_{st}^m = \mathbf{X}_{o,s}^T\mathbf{U}_{o,t} + \mathbf{X}_{o,t}^T\mathbf{U}_{o,s} \ , \ \varepsilon_{ss}^b = \mathbf{X}_{n,s}^T\mathbf{U}_{o,s} + \mathbf{X}_{o,s}^T\mathbf{U}_{n,s}$$

$$\varepsilon_{tt}^b = \mathbf{X}_{n,t}^T\mathbf{U}_{o,t} + \mathbf{X}_{o,t}^T\mathbf{U}_{n,t} \ , \ 2\varepsilon_{st}^b = \mathbf{X}_{n,s}^T\mathbf{U}_{o,t} + \mathbf{X}_{n,t}^T\mathbf{U}_{o,s} + \mathbf{X}_{o,s}^T\mathbf{U}_{n,t} + \mathbf{X}_{o,t}^T\mathbf{U}_{n,s}$$

and

$$\gamma_{\zeta s} = \mathbf{X}_n^T\mathbf{U}_{o,s} + \mathbf{X}_{o,s}^T\mathbf{U}_n \ , \ \gamma_{\zeta t} = \mathbf{X}_n^T\mathbf{U}_{o,t} + \mathbf{X}_{o,t}^T\mathbf{U}_n \tag{5b}$$

In the above expressions, "*m*" and "*b*" abbreviate "membrane" and "bending", respectively.

*2.4 Local Cartesian Coordinates* Material properties are often specified or defined with respect to a local Cartesian coordinate system whose x-y-plane is tangential to the mid-surface. At any point on the mid-surface, the unit vectors along the axes of any local system (x,y,z) can be expressed by :

$$\mathbf{e}_z = \frac{\mathbf{X}_{o,s} \times \mathbf{X}_{o,t}}{\left\|\mathbf{X}_{o,s} \times \mathbf{X}_{o,t}\right\|} \ , \ \mathbf{e}_x = \frac{\mathbf{v}_{ref} \times \mathbf{e}_z}{\left\|\mathbf{v}_{ref} \times \mathbf{e}_z\right\|} \ , \ \mathbf{e}_y = \mathbf{e}_z \times \mathbf{e}_x \tag{6}$$

In the definition, the reference vector $\mathbf{v}_{ref}$ is most conveniently taken to be an inplane principal material direction. For isotropic materials, we simply assume $\mathbf{v}_{ref} = \mathbf{X}_{o2} - \mathbf{X}_{o1}$. As $\mathbf{X}_n$ is parallel to or approximately parallel to $\mathbf{e}_z$, we have

$$\left[\begin{matrix} x_{,s} & x_{,t} & x_{,\zeta} \\ y_{,s} & y_{,t} & y_{,\zeta} \\ z_{,s} & z_{,t} & z_{,\zeta} \end{matrix}\right]\Bigg|_{\zeta=0} = \begin{bmatrix} \mathbf{e}_x^T \\ \mathbf{e}_y^T \\ \mathbf{e}_z^T \end{bmatrix}\begin{bmatrix} \mathbf{X}_{o,s} & \mathbf{X}_{o,t} & \mathbf{X}_n \end{bmatrix} \cong \begin{bmatrix} \mathbf{e}_x^T\mathbf{X}_{o,s} & \mathbf{e}_x^T\mathbf{X}_{o,t} & 0 \\ \mathbf{e}_y^T\mathbf{X}_{o,s} & \mathbf{e}_y^T\mathbf{X}_{o,t} & 0 \\ 0 & 0 & \mathbf{e}_z^T\mathbf{X}_n \end{bmatrix} \tag{7}$$

Owing to the vanishing nature of $x_{,\zeta}$, $y_{,\zeta}$, $z_{,s}$ and $z_{,t}$, the local Cartesian strain can be obtained as :

$$\boldsymbol{\varepsilon}^m = \begin{Bmatrix} \varepsilon_{xx}^m \\ \varepsilon_{yy}^m \\ 2\varepsilon_{xy}^m \end{Bmatrix} = \left[\begin{matrix} x_{,s}\,x_{,s} & y_{,s}\,y_{,s} & x_{,s}\,y_{,s} \\ x_{,t}\,x_{,t} & y_{,t}\,y_{,t} & x_{,t}\,y_{,t} \\ 2x_{,s}\,x_{,t} & 2y_{,s}\,y_{,t} & x_{,s}\,y_{,t}+x_{,t}\,y_{,s} \end{matrix}\right]^{-1}\Bigg|_{\zeta=0} \begin{Bmatrix} \varepsilon_{ss}^m \\ \varepsilon_{tt}^m \\ 2\varepsilon_{st}^m \end{Bmatrix} \tag{8a}$$

$$\boldsymbol{\varepsilon}^b = \begin{Bmatrix} \varepsilon^b_{xx} \\ \varepsilon^b_{yy} \\ 2\varepsilon^b_{xy} \end{Bmatrix} = \begin{bmatrix} x_{,s}\, x_{,s} & y_{,s}\, y_{,s} & x_{,s}\, y_{,s} \\ x_{,t}\, x_{,t} & y_{,t}\, y_{,t} & x_{,t}\, y_{,t} \\ 2x_{,s}\, x_{,t} & 2y_{,s}\, y_{,t} & x_{,s}\, y_{,t} + x_{,t}\, y_{,s} \end{bmatrix}^{-1}_{\zeta=0} \begin{Bmatrix} \varepsilon^b_{ss} \\ \varepsilon^b_{tt} \\ 2\varepsilon^b_{st} \end{Bmatrix} \tag{8b}$$

$$\boldsymbol{\gamma} = \begin{Bmatrix} \gamma_{zx} \\ \gamma_{zy} \end{Bmatrix} = \begin{bmatrix} z_{,\zeta}\, x_{,s} & z_{,\zeta}\, y_{,s} \\ z_{,\zeta}\, x_{,t} & z_{,\zeta}\, y_{,t} \end{bmatrix}^{-1}_{\zeta=0} \begin{Bmatrix} \gamma_{\zeta s} \\ \gamma_{\zeta t} \end{Bmatrix} \tag{8c}$$

By consolidating Eqn.(1b), Eqn.(3b), Eqn.(5) and Eqn.(8), the local Cartesian strains can be expressed in terms of the element displacement vector. Symbolically, we can write :

$$\boldsymbol{\varepsilon}^m = \mathbf{B}_m \mathbf{q} \quad , \quad \boldsymbol{\varepsilon}^b = \mathbf{B}_b \mathbf{q} \quad , \quad \boldsymbol{\gamma} = \mathbf{B}_\gamma \mathbf{q} \tag{9}$$

The element stiffness matrix is computed by integrating the strain energy over the element domain, i.e.

$$\mathbf{k} = \int_{-1}^{+1} \int_0^1 \int_0^{1-t} \left( (\mathbf{B}_m + \zeta \mathbf{B}_b)^T \mathbf{C}_\varepsilon (\mathbf{B}_m + \zeta \mathbf{B}_b) + \mathbf{B}_\gamma^T \mathbf{C}_\gamma \mathbf{B}_\gamma \right) J \, ds \, dt \, d\zeta \tag{10}$$

where $J$ is the Jacobian determinant for the transformation from $(X,Y,Z)$ to $(s,t,\zeta)$; $\mathbf{C}_\varepsilon$ and $\mathbf{C}_\gamma$ are the inplane plane stress and transverse shear material stiffness matrices, respectively. For isotropic materials,

$$\mathbf{C}_\varepsilon = \frac{E}{(1-\nu^2)} \begin{bmatrix} 1 & \nu & 0 \\ \nu & 1 & 0 \\ 0 & 0 & (1-\nu)/2 \end{bmatrix} \quad \text{and} \quad \mathbf{C}_\gamma = \frac{kE}{2(1+\nu)} \begin{bmatrix} 1 & 0 \\ 0 & 1 \end{bmatrix} \tag{11}$$

in which $E$ is elastic modulus, $\nu$ is the Poisson's ratio and $k$ is the shear correction factor commonly taken as 5/6. By adopting the conventional approximation of $J = J(\zeta=0)$, the element stiffness matrix can be simplified as :

$$\mathbf{k} = 2 \int_0^1 \int_0^{1-t} \left( \mathbf{B}_m^T \mathbf{C}_\varepsilon \mathbf{B}_m + \frac{1}{3} \mathbf{B}_b^T \mathbf{C}_\varepsilon \mathbf{B}_b + \mathbf{B}_\gamma^T \mathbf{C}_\gamma \mathbf{B}_\gamma \right) J(\zeta = 0) \, ds \, dt \tag{12}$$

It should be remarked that $\mathbf{C}_\varepsilon$ is a function of $\zeta$ for composite laminates. Thus, the bending and membrane energy may not be decoupled. The element stiffness matrix is rank sufficient when it is integrated by a three-point rules,

$$\mathbf{k}_{DISP} = \frac{1}{3}\sum_{i=I}^{III}(\mathbf{B}_{mi}^T\mathbf{C}_{\varepsilon i}\mathbf{B}_{mi} + \frac{1}{3}\mathbf{B}_{bi}^T\mathbf{C}_{\varepsilon i}\mathbf{B}_{bi} + \mathbf{B}_{ti}^T\mathbf{C}_{\gamma i}\mathbf{B}_{ti})J_i(\zeta = 0) \tag{13}$$

where *I*, *II* and *III* are the indices for the integration stations of the three-point rule. Their *s*-*t*-coordinates are *I*(1/6,1/6), *II*(2/3,1/6) and *III*(1/6,2/3).

## 3. OPTIMAL DIRECTIONAL DERIVATIVES

A generic subparametric triangle lying on the x-y-plane is considered. As the triangle can exactly interpolate the second order field, a generic third order field is considered :

$$f(x,y) = a_1x^3 + a_2x^2y + a_3xy^2 + a_4y^3 \tag{14}$$

where $a_i$'s are arbitrary constants. When the nodes are prescribed according to the above field, the interpolated field is :

$$\tilde{f} = \sum_{i=1}^{6} N_i(s,t)f(x_i,y_i) \tag{15}$$

After some straight forward but tedious mathematics, it is found that the x- and y-derivatives of $\tilde{f}$ are in general different from that of *f*. Nevertheless, the following categories of $\tilde{f}$ -derivative are identical to that of $f$ :

(category a) the derivatives along the element edges at the 2nd order quadrature points

(category b) the mean derivatives along the element medians (from a corner node to the midside node of the opposite edge)

(category c) the mean derivatives along the lines connecting nodes 4, 5 and 6

Thus, there are twelve directional derivatives identified to be exact for a third order field. As differentiation is always required in deriving strains from the displacement, the strain components

pertinent to the twelve derivatives are considered to be "optimal". In ANS6P [6] and the element to presented here, only the strains pertinent to (a) and (c) are adopted. In AST6, strains pertinent to (a) and (b) are employed [4].

## 4. DERIVING PHYSICAL STRAINS FROM THE OPTIMAL NATURAL STRAINS

Throughout the previous sections, only two area coordinates, namely, $r$ and $s$, are employed. There is another area coordinate $r$, see Fig.2a, whose relation with $s$ and $t$ is :

$$r + s + t = 1 \tag{16}$$

It can be noted that the directional derivatives in (category a) and (category c) are all along the lines of constant $r$-, $s$- or $t$-values. Along these lines, the following natural strains can be defined :

$$\widehat{\varepsilon}^m_{rr} = (\partial_r \mathbf{X}_o)^T(\partial_r \mathbf{U}_o),\ \widehat{\varepsilon}^b_{rr} = (\partial_r \mathbf{X}_n)^T(\partial_r \mathbf{U}_o) + (\partial_r \mathbf{X}_o)^T(\partial_r \mathbf{U}_n),\ \widehat{\gamma}_{\zeta r} = \mathbf{X}_n^T(\partial_r \mathbf{U}_o) + (\partial_r \mathbf{X}_o)^T \mathbf{U}_n \tag{17a}$$

$$\widehat{\varepsilon}^m_{ss} = (\partial_s \mathbf{X}_o)^T(\partial_s \mathbf{U}_o),\ \widehat{\varepsilon}^b_{ss} = (\partial_s \mathbf{X}_n)^T(\partial_s \mathbf{U}_o) + (\partial_s \mathbf{X}_o)^T(\partial_s \mathbf{U}_n),\ \widehat{\gamma}_{\zeta s} = \mathbf{X}_n^T(\partial_s \mathbf{U}_o) + (\partial_s \mathbf{X}_o)^T \mathbf{U}_n \tag{17b}$$

$$\widehat{\varepsilon}^m_{tt} = (\partial_t \mathbf{X}_o)^T(\partial_t \mathbf{U}_o),\ \widehat{\varepsilon}^b_{tt} = (\partial_t \mathbf{X}_n)^T(\partial_t \mathbf{U}_o) + (\partial_t \mathbf{X}_o)^T(\partial_t \mathbf{U}_n),\ \widehat{\gamma}_{\zeta t} = \mathbf{X}_n^T(\partial_t \mathbf{U}_o) + (\partial_t \mathbf{X}_o)^T \mathbf{U}_n \tag{17c}$$

where $\partial_r$, $\partial_s$ and $\partial_t$ when operate on a function $F = F(r, s, t)$ are defined as :

$$\partial_r F(r,s,t) = \frac{\partial F(r,s,1-r-s)}{\partial r},\ \partial_s F(r,s,t) = \frac{\partial F(1-s-t,s,t)}{\partial s},\ \partial_t F(r,s,t) = \frac{\partial F(r,1-t-r,t)}{\partial t} \tag{18}$$

In subparametric elements, the natural strains in Eqn.(17a), Eqn.(17b) and Eqn.(17c) are parallel to the line joining node 3 and node 1, the line joining node 1 and node 2, and the line joining node 2 and node 3, respectively.

*4.1 Assumed Natural Membrane and Bending Strains* A major concern of selecting the membrane strains is membrane locking that often appears in the thin and curved standard elements. Similar to shear locking [1,3,4,15], an effective way of alleviating membrane locking is to employ membrane strains sampled at and along the element edges as in (category a). Since these strains are common to the adjacent elements, the number of independent membrane strain samples and thus the number of numerical penalties to enforce zero membrane strains in the global level can be reduced. To this light, membrane locking can be alleviated.

For the six-node element, nine membrane strains and nine bending strains must be sampled or the element will be rank deficient. Hence, the strains corresponding to (category a) and (category b) provide the right number of optimal samples. The optimal natural membrane and bending strains corresponding to (category a) are :

$$\widehat{\varepsilon}_{rr}^{m-} = \widehat{\varepsilon}_{rr}^{m}(r=\frac{1}{2}-\frac{1}{2\sqrt{3}}, s=0),\ \widehat{\varepsilon}_{ss}^{m-} = \widehat{\varepsilon}_{ss}^{m}(s=\frac{1}{2}-\frac{1}{2\sqrt{3}}, t=0),\ \widehat{\varepsilon}_{tt}^{m-} = \widehat{\varepsilon}_{tt}^{m}(t=\frac{1}{2}-\frac{1}{2\sqrt{3}}, r=0) \quad (19a)$$

$$\widehat{\varepsilon}_{rr}^{m+} = \widehat{\varepsilon}_{rr}^{m}(r=\frac{1}{2}+\frac{1}{2\sqrt{3}}, s=0),\ \widehat{\varepsilon}_{ss}^{m+} = \widehat{\varepsilon}_{ss}^{m}(s=\frac{1}{2}+\frac{1}{2\sqrt{3}}, t=0),\ \widehat{\varepsilon}_{tt}^{m+} = \widehat{\varepsilon}_{tt}^{m}(t=\frac{1}{2}+\frac{1}{2\sqrt{3}}, r=0) \quad (19b)$$

$$\widehat{\varepsilon}_{rr}^{b-} = \widehat{\varepsilon}_{rr}^{b}(r=\frac{1}{2}-\frac{1}{2\sqrt{3}}, s=0),\ \widehat{\varepsilon}_{ss}^{b-} = \widehat{\varepsilon}_{ss}^{b}(s=\frac{1}{2}-\frac{1}{2\sqrt{3}}, t=0),\ \widehat{\varepsilon}_{tt}^{b-} = \widehat{\varepsilon}_{tt}^{b}(t=\frac{1}{2}-\frac{1}{2\sqrt{3}}, r=0) \quad (19c)$$

$$\widehat{\varepsilon}_{rr}^{b+} = \widehat{\varepsilon}_{rr}^{b}(r=\frac{1}{2}+\frac{1}{2\sqrt{3}}, s=0),\ \widehat{\varepsilon}_{ss}^{b+} = \widehat{\varepsilon}_{ss}^{b}(s=\frac{1}{2}+\frac{1}{2\sqrt{3}}, t=0),\ \widehat{\varepsilon}_{tt}^{b+} = \widehat{\varepsilon}_{tt}^{b}(t=\frac{1}{2}+\frac{1}{2\sqrt{3}}, r=0) \quad (19d)$$

As the membrane strains are second order functions of the natural coordinates, the membrane and bending strains corresponding to (category c) can be calculated by using the second order quadrature, i.e.

$$\widehat{\varepsilon}_{rr}^{ma} = \frac{1}{2}\widehat{\varepsilon}_{rr}^{m}(r=\frac{1}{4}-\frac{1}{4\sqrt{3}}, s=\frac{1}{2})+\frac{1}{2}\widehat{\varepsilon}_{rr}^{m}(r=\frac{1}{4}+\frac{1}{4\sqrt{3}}, s=\frac{1}{2}) \quad (20a)$$

$$\widehat{\varepsilon}_{ss}^{ma} = \frac{1}{2}\widehat{\varepsilon}_{ss}^{m}(s=\frac{1}{4}-\frac{1}{4\sqrt{3}}, t=\frac{1}{2})+\frac{1}{2}\widehat{\varepsilon}_{ss}^{m}(s=\frac{1}{4}+\frac{1}{4\sqrt{3}}, t=\frac{1}{2}) \quad (20b)$$

$$\widehat{\varepsilon}_{tt}^{ma} = \frac{1}{2}\widehat{\varepsilon}_{tt}^{m}(t=\frac{1}{4}-\frac{1}{4\sqrt{3}}, r=\frac{1}{2})+\frac{1}{2}\widehat{\varepsilon}_{tt}^{m}(t=\frac{1}{4}+\frac{1}{4\sqrt{3}}, r=\frac{1}{2}) \quad (20c)$$

$$\widehat{\varepsilon}_{rr}^{ba} = \frac{1}{2}\widehat{\varepsilon}_{rr}^{b}(r=\frac{1}{4}-\frac{1}{4\sqrt{3}}, s=\frac{1}{2})+\frac{1}{2}\widehat{\varepsilon}_{rr}^{b}(r=\frac{1}{4}+\frac{1}{4\sqrt{3}}, s=\frac{1}{2}) \quad (20d)$$

$$\widehat{\varepsilon}_{ss}^{ba} = \frac{1}{2}\widehat{\varepsilon}_{ss}^{b}(s=\frac{1}{4}-\frac{1}{4\sqrt{3}}, t=\frac{1}{2})+\frac{1}{2}\widehat{\varepsilon}_{ss}^{b}(s=\frac{1}{4}+\frac{1}{4\sqrt{3}}, t=\frac{1}{2}) \quad (20e)$$

$$\widehat{\varepsilon}_{tt}^{ba} = \frac{1}{2}\widehat{\varepsilon}_{tt}^{b}(t=\frac{1}{4}-\frac{1}{4\sqrt{3}}, r=\frac{1}{2})+\frac{1}{2}\widehat{\varepsilon}_{tt}^{b}(t=\frac{1}{4}+\frac{1}{4\sqrt{3}}, r=\frac{1}{2}) \quad (20f)$$

By taking the sampling locations of the above average strains at the mid-points of the lines concerned, the interpolated natural strains are derived to be :

$$\widetilde{\varepsilon}_{rr}^{m} = g_1(r,s)\widehat{\varepsilon}_{rr}^{m-} + g_2(r,s)\widehat{\varepsilon}_{rr}^{m+} + 2s\widehat{\varepsilon}_{rr}^{ma},\ \widetilde{\varepsilon}_{rr}^{b} = g_1(r,s)\widehat{\varepsilon}_{rr}^{b-} + g_2(r,s)\widehat{\varepsilon}_{rr}^{b+} + 2s\widehat{\varepsilon}_{rr}^{ba} \quad (21a)$$

$$\tilde{\varepsilon}_{ss}^{m} = g_1(s,t)\hat{\varepsilon}_{ss}^{m-} + g_2(s,t)\hat{\varepsilon}_{ss}^{m+} + 2t\hat{\varepsilon}_{ss}^{ma} \;,\; \tilde{\varepsilon}_{ss}^{b} = g_1(s,t)\hat{\varepsilon}_{ss}^{b-} + g_2(s,t)\hat{\varepsilon}_{ss}^{b+} + 2t\hat{\varepsilon}_{ss}^{ba} \quad (21b)$$

$$\tilde{\varepsilon}_{tt}^{m} = g_1(t,r)\hat{\varepsilon}_{tt}^{m-} + g_2(t,r)\hat{\varepsilon}_{tt}^{m+} + 2r\hat{\varepsilon}_{tt}^{ma} \;,\; \tilde{\varepsilon}_{tt}^{b} = g_1(t,r)\hat{\varepsilon}_{tt}^{b-} + g_2(t,r)\hat{\varepsilon}_{tt}^{b+} + 2r\hat{\varepsilon}_{tt}^{ba} \quad (21c)$$

where

$$g_1(\xi,\eta) = (\frac{1}{2}+\frac{\sqrt{3}}{2}) - \xi\sqrt{3} - (1+\frac{\sqrt{3}}{2})\eta \;,\; g_2(\xi,\eta) = (\frac{1}{2}-\frac{\sqrt{3}}{2}) + \xi\sqrt{3} - (1-\frac{\sqrt{3}}{2})\eta$$

*4.2 Physical Membrane and Bending Strains* Following the derivation to that of Eqn.(8), the physical membrane and bending strain components can be derived from the above equations :

$$\begin{Bmatrix} \tilde{\varepsilon}_{xx}^{m} \\ \tilde{\varepsilon}_{yy}^{m} \\ 2\tilde{\varepsilon}_{xy}^{m} \end{Bmatrix} = \begin{bmatrix} (\partial_r x)^2 & (\partial_r y)^2 & (\partial_r x)(\partial_r y) \\ (\partial_s x)^2 & (\partial_s y)^2 & (\partial_s x)(\partial_s y) \\ (\partial_t x)^2 & (\partial_t y)^2 & (\partial_t x)(\partial_t y) \end{bmatrix}_{\zeta=0}^{-1} \begin{Bmatrix} \tilde{\varepsilon}_{rr}^{m} \\ \tilde{\varepsilon}_{ss}^{m} \\ \tilde{\varepsilon}_{tt}^{m} \end{Bmatrix} \quad (22a)$$

$$\begin{Bmatrix} \tilde{\varepsilon}_{xx}^{b} \\ \tilde{\varepsilon}_{yy}^{b} \\ 2\tilde{\varepsilon}_{xy}^{b} \end{Bmatrix} = \begin{bmatrix} (\partial_r x)^2 & (\partial_r y)^2 & (\partial_r x)(\partial_r y) \\ (\partial_s x)^2 & (\partial_s y)^2 & (\partial_s x)(\partial_s y) \\ (\partial_t x)^2 & (\partial_t y)^2 & (\partial_t x)(\partial_t y) \end{bmatrix}_{\zeta=0}^{-1} \begin{Bmatrix} \tilde{\varepsilon}_{rr}^{b} \\ \tilde{\varepsilon}_{ss}^{b} \\ \tilde{\varepsilon}_{tt}^{b} \end{Bmatrix} \quad (22b)$$

in which

$$\partial_r x = \mathbf{e}_x^T(\partial_r \mathbf{X}_o) \;,\; \partial_r y = \mathbf{e}_y^T(\partial_r \mathbf{X}_o) \;,\; \partial_s x = \mathbf{e}_x^T(\partial_s \mathbf{X}_o)$$

$$\partial_s y = \mathbf{e}_y^T(\partial_s \mathbf{X}_o) \;,\; \partial_t x = \mathbf{e}_x^T(\partial_t \mathbf{X}_o) \;,\; \partial_t y = \mathbf{e}_y^T(\partial_t \mathbf{X}_o)$$

*4.3 Assumed Natural Shear Strain* For the six-node element, six transverse shear strains must be sampled or the element will be rank deficient. As a matter of fact, the six edge transverse shear strains (category a) are employed by the plate bending element TRI-6 [3]. However, the element appears to be too flexible and this is also reflected by its large constraint ratio CR which equals two [4,15]. The MITC7 plate bending elements also employ the six edge transverse shear strain but its CR is lowered to 1.6 by including two sampled transverse shear strain inside the element. Unfortunately, MITC7's have to be evaluated by the expensive seven point integrated rule.

In our previous AST6, the six edge transverse shear strains (category a) are combined to form three mean edge transverse shear strains so as to avoid an overly flexible element. To secure the full element rank, the three mean median transverse shear strains (category b) are also employed in AST6 which ends up with its CR equal to 4/3 [4].

The shear strain field to be adopted here has been used in ANS6P [6]. Similar to the optimal membrane and bending strains, the optimal shear strains corresponding to category (a) are :

$$\hat{\gamma}^{-}_{\zeta r} = \hat{\gamma}_{\zeta r}(r = \frac{1}{2} - \frac{1}{2\sqrt{3}}, s = 0) \ , \ \hat{\gamma}^{+}_{\zeta r} = \hat{\gamma}_{\zeta r}(r = \frac{1}{2} + \frac{1}{2\sqrt{3}}, s = 0) \tag{23a}$$

$$\hat{\gamma}^{-}_{\zeta s} = \gamma_{\zeta s}(s = \frac{1}{2} - \frac{1}{2\sqrt{3}}, t = 0) \ , \ \hat{\gamma}^{+}_{\zeta s} = \hat{\gamma}_{\zeta s}(s = \frac{1}{2} + \frac{1}{2\sqrt{3}}, t = 0) \tag{23b}$$

$$\hat{\gamma}^{-}_{\zeta t} = \hat{\gamma}_{\zeta t}(t = \frac{1}{2} - \frac{1}{2\sqrt{3}}, r = 0) \ , \ \hat{\gamma}^{+}_{\zeta t} = \hat{\gamma}_{\zeta t}(t = \frac{1}{2} + \frac{1}{2\sqrt{3}}, r = 0) \tag{23c}$$

as depicted in Fig.2c. Noting that the natural shear strains are third order functions of the natural coordinates, the three shear strains corresponding to (category c) of the last section can also be computed by using the second order quadrature. They are :

$$\hat{\gamma}^{a}_{\zeta r} = \frac{1}{2}\hat{\gamma}_{\zeta r}(r = \frac{1}{4} - \frac{1}{4\sqrt{3}}, s = \frac{1}{2}) + \frac{1}{2}\hat{\gamma}_{\zeta r}(r = \frac{1}{4} + \frac{1}{4\sqrt{3}}, s = \frac{1}{2}) \tag{24a}$$

$$\hat{\gamma}^{a}_{\zeta s} = \frac{1}{2}\hat{\gamma}_{\zeta s}(s = \frac{1}{4} - \frac{1}{4\sqrt{3}}, t = \frac{1}{2}) + \frac{1}{2}\hat{\gamma}_{\zeta s}(s = \frac{1}{4} + \frac{1}{4\sqrt{3}}, t = \frac{1}{2}) \tag{24b}$$

$$\hat{\gamma}^{a}_{\zeta t} = \frac{1}{2}\hat{\gamma}_{\zeta t}(t = \frac{1}{4} - \frac{1}{4\sqrt{3}}, r = \frac{1}{2}) + \frac{1}{2}\hat{\gamma}_{\zeta t}(t = \frac{1}{4} + \frac{1}{4\sqrt{3}}, r = \frac{1}{2}) \tag{24c}$$

Similar to the membrane and bending natural strains, the interpolated natural shear strains are :

$$\tilde{\gamma}_{\zeta r} = g_1(r,s)\hat{\gamma}^{-}_{\zeta r} + g_2(r,s)\hat{\gamma}^{+}_{\zeta r} + 2s\hat{\gamma}^{a}_{\zeta r} \ , \ \tilde{\gamma}_{\zeta s} = g_1(s,t)\hat{\gamma}^{-}_{\zeta s} + g_2(s,t)\hat{\gamma}^{+}_{\zeta s} + 2t\hat{\gamma}^{a}_{\zeta s} \ ,$$
$$\tilde{\gamma}_{\zeta t} = g_1(t,r)\hat{\gamma}^{-}_{\zeta t} + g_2(t,r)\hat{\gamma}^{+}_{\zeta t} + 2r\hat{\gamma}^{a}_{\zeta t} \tag{25}$$

in which functions $g_1$ and $g_2$ have been defined in Eqn.(21).

*4.4 Physical Shear Strain* An interpolated linear physical transverse shear strain field which consists of two components $\gamma_{zx}$ and $\gamma_{zy}$ can be derived based on any two of $\tilde{\gamma}_{\zeta r}$, $\tilde{\gamma}_{\zeta s}$ and $\tilde{\gamma}_{\zeta t}$. When this is done, there is a severe sensitivity towards different node numbering sequence [16]. Fortunately, only the physical strains at the integration stations are required for computing the element stiffness matrix at the first instant. To circumvent the sensitivity, the scheme for deriving the interpolated physical strains portrayed in Fig.2d is devised. At integration stations *I*, *II* and *III*,

$\tilde{\gamma}_{\zeta t}$, $\tilde{\gamma}_{\zeta r}$ and $\tilde{\gamma}_{\zeta s}$ are not employed, respectively. This cyclic symmetric scheme can eliminate the sensitivity and this point has also been confirmed by numerical tests. Following the similar derivation to that for Eqn.(8) and making use of the interpolated strains in Eqn.(25), the physical strains at the integration stations are worked out to be :

$$\begin{Bmatrix}\tilde{\gamma}_{zx}\\ \tilde{\gamma}_{zy}\end{Bmatrix}_I = \begin{bmatrix} z_{,\zeta}\,\partial_r x & z_{,\zeta}\,\partial_r y \\ z_{,\zeta}\,\partial_s x & z_{,\zeta}\,\partial_s y \end{bmatrix}^{-1}_{I,\zeta=0} \begin{Bmatrix}\tilde{\gamma}_{\zeta r}\\ \tilde{\gamma}_{\zeta s}\end{Bmatrix}_I = \begin{bmatrix} z_{,\zeta}\,\partial_r x & z_{,\zeta}\,\partial_r y \\ z_{,\zeta}\,\partial_s x & z_{,\zeta}\,\partial_s y \end{bmatrix}^{-1}_{I,\zeta=0} \begin{Bmatrix}\alpha_1\gamma^{-}_{\zeta r} + \alpha_2\gamma^{+}_{\zeta r} + \gamma^{a}_{\zeta r}/3\\ \alpha_2\gamma^{-}_{\zeta s} + \alpha_1\gamma^{+}_{\zeta s} + \gamma^{a}_{\zeta s}/3\end{Bmatrix} \quad (26a)$$

$$\begin{Bmatrix}\tilde{\gamma}_{zx}\\ \tilde{\gamma}_{zy}\end{Bmatrix}_{II} = \begin{bmatrix} z_{,\zeta}\,\partial_s x & z_{,\zeta}\,\partial_s y \\ z_{,\zeta}\,\partial_t x & z_{,\zeta}\,\partial_t y \end{bmatrix}^{-1}_{II,\zeta=0} \begin{Bmatrix}\tilde{\gamma}_{zs}\\ \tilde{\gamma}_{zt}\end{Bmatrix}_{II} = \begin{bmatrix} z_{,\zeta}\,\partial_s x & z_{,\zeta}\,\partial_s y \\ z_{,\zeta}\,\partial_t x & z_{,\zeta}\,\partial_t y \end{bmatrix}^{-1}_{II,\zeta=0} \begin{Bmatrix}\alpha_1\gamma^{-}_{\zeta s} + \alpha_2\gamma^{+}_{\zeta s} + \gamma^{a}_{\zeta s}/3\\ \alpha_2\gamma^{-}_{\zeta t} + \alpha_1\gamma^{+}_{\zeta t} + \gamma^{a}_{\zeta t}/3\end{Bmatrix} \quad (26b)$$

$$\begin{Bmatrix}\tilde{\gamma}_{zx}\\ \tilde{\gamma}_{zy}\end{Bmatrix}_{III} = \begin{bmatrix} z_{,\zeta}\,\partial_t x & z_{,\zeta}\,\partial_t y \\ z_{,\zeta}\,\partial_r x & z_{,\zeta}\,\partial_r y \end{bmatrix}^{-1}_{III,\zeta=0} \begin{Bmatrix}\gamma_{zt}\\ \gamma_{zr}\end{Bmatrix}_{III} = \begin{bmatrix} z_{,\zeta}\,\partial_t x & z_{,\zeta}\,\partial_t y \\ z_{,\zeta}\,\partial_r x & z_{,\zeta}\,\partial_r y \end{bmatrix}^{-1}_{III,\zeta=0} \begin{Bmatrix}\alpha_1\gamma^{-}_{\zeta t} + \alpha_2\gamma^{+}_{\zeta t} + \gamma^{a}_{\zeta t}/3\\ \alpha_2\gamma^{-}_{\zeta r} + \alpha_1\gamma^{+}_{\zeta r} + \gamma^{a}_{\zeta r}/3\end{Bmatrix} \quad (26c)$$

where

$$\alpha_1 = (4-3\sqrt{3})/12 \ , \ \alpha_2 = (4+3\sqrt{3})/12$$

and the matrix entries have been defined in Eqn.(7) and Eqn.(22). With the above strains at the integration stations, the physical shear strain field can be obtained by interpolation.

## 5. ASSUMED NATURAL STRAIN SIX-NODE SHELL ELEMENT

In the last section, the physical membrane and bending strain fields have been derived in Eqn.(22) whereas the physical shear strains at the integration stations are derived at Eqn.(16). If these equations are expressed symbolically as :

$$\begin{Bmatrix}\tilde{\varepsilon}^{m}_{xx}\\ \tilde{\varepsilon}^{m}_{yy}\\ 2\tilde{\varepsilon}^{m}_{xy}\end{Bmatrix} = \tilde{\mathbf{B}}_m\,\mathbf{q} \ , \ \begin{Bmatrix}\tilde{\varepsilon}^{b}_{xx}\\ \tilde{\varepsilon}^{b}_{yy}\\ 2\tilde{\varepsilon}^{b}_{xy}\end{Bmatrix} = \tilde{\mathbf{B}}_b\,\mathbf{q} \ , \ \begin{Bmatrix}\tilde{\gamma}_{zx}\\ \tilde{\gamma}_{zy}\end{Bmatrix}_I = \tilde{\mathbf{B}}_{\gamma I}\,\mathbf{q} \ , \ \begin{Bmatrix}\tilde{\gamma}_{zx}\\ \tilde{\gamma}_{zy}\end{Bmatrix}_{II} = \tilde{\mathbf{B}}_{\gamma II}\,\mathbf{q} \ , \ \begin{Bmatrix}\tilde{\gamma}_{zx}\\ \tilde{\gamma}_{zy}\end{Bmatrix}_{III} = \tilde{\mathbf{B}}_{\gamma III}\,\mathbf{q} \quad (27)$$

With them replacing the ones in Eqn.(13), a new element stiffness matrix is formed :

$$\mathbf{k}_{ANS6S} = \frac{1}{3}\sum_{i=I}^{III}(\tilde{\mathbf{B}}^{T}_{mi}\mathbf{C}_{\varepsilon i}\tilde{\mathbf{B}}_{mi} + \frac{1}{3}\tilde{\mathbf{B}}^{T}_{bi}\mathbf{C}_{\varepsilon i}\tilde{\mathbf{B}}_{bi} + \tilde{\mathbf{B}}^{T}_{\gamma i}\mathbf{C}_{\gamma i}\tilde{\mathbf{B}}_{\gamma i})J_i(\zeta=0) \quad (28)$$

This assumed natural strain six-node shell element will be termed ANS6S.

## 6. NUMERICAL BENCHMARK PROBLEMS

In this section, popular numerical benchmark tests will be examined by the conventional six-node element DISP and the proposed assumed natural strain element ANS6S. For plate bending problems, the results of MITC7 [2] and AST6 [4] are also included as far as possible. Unless specified, all finite element predictions are normalized by the reference solutions of MacNeal & Harder [17].

*6.1 Patch Test and Rank Examination* It has been tested that both DISP and ANS6S pass the moment, membrane stress and transverse shear stress patch tests prescribed by MacNeal & Harder [17]. Moreover, both elements have only six zero eigenvectors which correspond to the six rigid body modes.

*6.2 Shear Locking Test : Clamped Square Plate subjected to Central Point Load* A quadrant of a square plate is modelled by 2×2 mesh (8 elements) and 4×4 meshes (32 elements), see Fig.3. Along the supported edges, all d.o.f.s are restrained. The plate is subjected to a central point load and its side length ($L$) to thickness ($h$) ratio is varied. The central deflections normalized by the solution given in the textbook of Timoshenko & Woinowsky-Krieger [18] are listed in Table 1. Only DISP exhibits shear locking.

Table 1. Normalized central deflections for fully clamped square plate subjected to central point load, see Fig.3

| | 2 × 2 mesh | | | 4 × 4 mesh | | |
|---|---|---|---|---|---|---|
| L/h | T6/3 | AST6 | ANS6S | T6/3 | AST6 | ANS6S |
| $10^2$ | 0.304 | 0.872 | 0.936 | 0.747 | 0.998 | 1.008 |
| $10^3$ | $5.2\text{x}10^{-3}$ | 0.712 | 0.880 | 0.355 | 0.983 | 0.988 |
| $10^4$ | $5.2\text{x}10^{-5}$ | 0.707 | 0.879 | $9.4\text{x}10^{-3}$ | 0.981 | 0.987 |
| $10^5$ | $5.2\text{x}10^{-7}$ | 0.707 | 0.879 | $9.6\text{x}10^{-5}$ | 0.981 | 0.987 |

*6.3 Membrane Locking Test : Twisted Beam Problem* Fig.4 depicts a $90^o$ pre-twisted beam which resembles a turbine blade. At its clamped end, all nodal d.o.f s are restrained. In-plane and out-of-plane end forces are applied to the free end. This is often considered to be a good test for membrane locking [19]. The end deflections for different mesh densities and thickness normalized by the reference solutions given in reference [19] are tabulated in Table 2. Unlike DISP, ANS6S shows no sign of membrane locking.

Table 2. Normalized end deflections for twisted beam, see Fig.4

| loading | inplane | | | | out-of-plane | | | |
|---|---|---|---|---|---|---|---|---|
| thickness | 0.32 | | 0.0032 | | 0.32 | | 0.0032 | |
| nodes/side | 3 × 13 | 5 × 25 | 3 × 13 | 5 × 25 | 3 × 13 | 5 × 25 | 3 × 13 | 5 × 25 |

| | | | | | | | | |
|---|---|---|---|---|---|---|---|---|
| DISP | 0.972 | 0.995 | 0.018 | 0.069 | 0.973 | 0.997 | 0.022 | 0.068 |
| ANS6S | 0.997 | 0.998 | 0.992 | 0.990 | 0.996 | 0.999 | 1.000 | 0.994 |

*6.4 Circular Plates* A circular plate of radius $R$ to thickness ratio equal to 500 is considered. A quadrant of the plate is modelled by 6, 24 and 96 elements, see Fig.5. Both simply supported ($w = 0$) and fully clamped ($w = \theta_1 = \theta_2 = 0$) conditions are attempted. The normalized central deflections and bending moments are listed in Tables 3a and 3b. In the simply supported problems, ANS6P has a higher coarse-mesh accuracy than MITC7 whereas ANS6S appears to be more accurate than AST6 in the clamped problems.

Finally, the deflections along the x-axis for the fully-clamped and centrally point-loaded plate with $R/h$ equal to 500 and 5 are computed by using the 24 element mesh. The results shown in Table 3c have been normalized by the thick plate solution [19] :

$$w = \frac{PR^2}{16\pi D}\left(1 - \frac{r^2}{R^2} + \frac{2r^2}{R^2}\ln(\frac{r}{R}) - \frac{8D}{kGhr^2}\ln(\frac{r}{R})\right)$$

ANS6S is more accurate than AST6 in this problem. More plate bending problems are reported in reference [6]. Overall speaking, ANS6S yields marginally higher accuracy than the previously proposed AST6 assumed strain element.

Table 3a. Normalized deflections for circular plate, see Fig.5

| model | no. of elements | central point load | | uniform pressure | |
|---|---|---|---|---|---|
| | | simply supported | fully clamped | simply supported | fully clamped |
| DISP | 3 | 0.391 | 0.039 | 0.884 | 0.086 |
| | 12 | 0.932 | 0.563 | 0.971 | 0.462 |
| | 48 | 0.977 | 0.897 | 0.992 | 0.889 |
| AST6 | 6 | 0.991 | 0.970 | 0.994 | 0.977 |
| | 24 | 0.997 | 0.968 | 1.000 | 0.957 |
| | 96 | 0.999 | 0.981 | 1.000 | 0.967 |
| ANS6S | 6 | 1.004 | 0.972 | 1.016 | 1.043 |
| | 24 | 1.001 | 0.995 | 1.002 | 1.008 |
| | 96 | 1.001 | 1.001 | 1.002 | 1.004 |
| MITC7 | 6 | 0.987 | 0.980[+] | —— | —— |
| | 24 | 0.996 | 0.992[+] | —— | —— |
| | 96 | 0.999 | 0.998[+] | —— | —— |

[+] it is not specified in reference [2] whether the fully or partially clamped condition is employed

Table 3b. Normalized central bending moments for circular plate under uniform pressure, see Fig.5

| model | no. of elements | simply supported | fully clamped |
|---|---|---|---|
| DISP | 6 | 1.008 | -0.157 |
| | 24 | 0.934 | 0.362 |
| | 96 | 0.971 | 0.907 |
| AST6 | 6 | 1.056 | 1.171 |
| | 24 | 1.018 | 1.034 |
| | 96 | 1.005 | 0.996 |
| ANS6S | 6 | 1.076 | 1.172 |
| | 24 | 1.021 | 1.037 |

| | | | |
|---|---|---|---|
| | 96 | 1.000 | 1.004 |

Table 3c. Normalized deflection for thin/thick circular plate under central point load, see Fig.5

| *r/R* | model | 1/8 | 2/8 | 3/8 | 4/8 | 5/8 | 6/8 | 7/8 |
|---|---|---|---|---|---|---|---|---|
| 500 | T6/3 | 0.581 | 0.573 | 0.533 | 0.492 | 0.449 | 0.437 | 0.524 |
| | AST6 | 0.972 | 0.964 | 0.957 | 0.941 | 0.923 | 0.825 | 0.968 |
| | ANS6S | 1.007 | 1.004 | 1.004 | 1.010 | 1.021 | 1.050 | 1.097 |
| 5 | T6/3 | 1.010 | 0.992 | 0.993 | 0.994 | 1.003 | 0.992 | 1.047 |
| | AST6 | 1.034 | 1.017 | 1.019 | 1.025 | 1.039 | 1.035 | 1.080 |
| | ANS6S | 1.033 | 1.017 | 1.020 | 1.029 | 1.039 | 1.038 | 1.006 |

6.5 *Cantilever subjected End Forces* This problem is taken from MacNeal's textbook [20]. Two meshes are used to model the cantilever in Fig.6. While the first mesh is subparametric as shown in Fig.6a, the second mesh is obtained by shifting the nodes insides the four isosceles trapezoids to the respective centres. The end deflections normalized by the thin beam theory are given in Table 4. While both elements yield the same result with the subparametric mesh, sharp difference is observed with the non-subparametric mesh.

Table 4. Normalized end deflections for cantilever, see Fig.6

| element model | subparametric mesh | non-subparametric mesh |
|---|---|---|
| DISP | 0.962 | 0.460 |
| ANS6S | 0.962 | 0.839 |

*6.6 Curved Beam* The curved beam is portrayed in Fig.7. The beam is of unit thickness and fully clamped at the supported end. At the free end, in-plane and out-of-plane forces are applied. The normalized end deflections along the loading directions are tabulated in Table 5. The elements with the assumed membrane strain field yield the best accuracy for the in-plane loading. As the beam is quite thick and thus locking is not a concern, all elements are of the same accuracy for the out-of-plane loading.

Table 5. Normalized tip deflections for curved beam, see Fig.7

| element model | inplane loading | out-of-plane loading |
|---|---|---|
| DISP | 0.951 | 0.954 |
| ANS6S | 1.000 | 0.963 |

*6.7 Hemispherical Shell* A hemispherical shell with a $18^o$ cut-out is subjected to anti-symmetric point loads at its bottom. Owing to symmetry, a quarter of this doubly-curved shell problem is modelled, see Fig.8. Radial deflections for different mesh densities at the points of loading are normalized by the reference solution 0.0924 [17] and listed in Table 6. ANS6S is much more accurate than DISP.

Table 6. Normalized tip deflections for hemispherical shell, Fig.8

| nodes/side | 5 | 9 | 13 | 17 |
|---|---|---|---|---|

| | | | | |
|---|---|---|---|---|
| DISP | 0.008 | 0.055 | 0.175 | 0.370 |
| ANS6S | 0.949 | 0.982 | 0.995 | 1.001 |

*6.8 Scordelis-Lo Roof* This problem is depicted in Fig.9. The shell is loaded by its own weight specified as $g$ unit force per unit mid-surface area. The roof is mounted on two rigid end diaphragms over which $u = w = \theta_y$. The two longitudinal edges remain free-hanging. Only a quarter of the roof is analyzed due to symmetry. The vertical deflections at point A are computed and normalized as listed in Table 7. Again, ANS6S is more accurate.

Table 7. Normalized tip deflections for the Scordelis-Lo roof, Fig.9

| Nodes/side | 3 | 5 | 7 | 9 | 13 | 17 |
|---|---|---|---|---|---|---|
| DISP | 0.263 | 0.435 | 0.692 | 0.846 | 0.951 | 0.978 |
| ANS6S | 0.856 | 0.825 | 0.952 | 0.982 | 0.993 | 0.995 |

*6.9 Pinched cylinder* The thin cylinder depicted in Fig.10 is subjected to diametrically opposite point loads. The cylinder is supported by two rigid end diaphragms over which $u = w = \theta_y$. Owing to symmetry, one octant of the cylinder is modelled. The predicted deflections under the point load are normalized as in Table 10. Once again, ANS6S is more accurate.

Table 8. Normalized tip deflections for a pinched cylinder, see Fig.10

| nodes/side | 5 | 7 | 9 | 13 | 17 |
|---|---|---|---|---|---|
| DISP | 0.109 | 0.175 | 0.281 | 0.502 | 0.675 |
| ANS6S | 0.502 | 0.741 | 0.857 | 0.955 | 0.985 |

## 7. CLOSURE

ANS6S assumed natural strain $C^0$ curved shell element is developed. To our best knowledge, it is the first assumed natural strain quadratic triangular shell element. As illustrated by ad hoc tests for locking, the present assumed natural membrane and shear strain fields effectively overcome the membrane and shear locking, respectively. Moreover, ANS6S is distinctively more accurate than its displacement counterpart DISP.

**Acknowledgment** - The financial support of *Hong Kong Research Grant Council* in the form of an *Earmarked Grant* is gratefully acknowledged.

## REFERENCES

1. O.C.Zienkiewicz, D.Lefebvre, "A robust triangular plate bending element of the Reissner-Mindlin type", *Inter.J.Numer.Methods Engrg*., **26**, 1169-1184 (1988)

2. K.J.Bathe, F.Brezzi, S.W.Cho, "The MITC7 and MITC9 plate bending element", *Computers & Structures*, **32**, 797-814 (1989)

3. O.C.Zienkiewicz, R.L.Taylor, P.Papadopoulos, E.Onate, "Plate bending elements with discrete constraints : new triangular elements", *Computers & Structures*, **35**, 505-522 (1990)

4. K.Y.Sze, D.Zhu, D.-P.Chen, "Quadratic Triangular $C^0$ Plate Bending Element", *Inter.J.Numer. Methods Engrg.*, **40**, 937-951 (1997)

5. K.Y.Sze, D.Zhu, "On the relative merits of three-point integration rules for six-node triangles", *Finite Elements in Analysis & Design*, **27**, 335-343 (1997)

6. K.Y.Sze, D.Zhu, "An quadratic assumed natural strain triangular element for plate bending analysis", *Commun.Numerical Methods Engrg.*, **14**, 1013-1025 (1998)

7. Chaudhuri, R.A., "Degenerate triangular shell element with constant cross-sectional warping", *Computers & Structures*, **28**, *315-325* (1988)

8. F.Keulen, A.Bout, L.J.Ernst, "Nonlinear thin shell analysis using a curved triangular element", *Computer Methods Appl.Mech.Engrg.*, **103**, 315-343 (1993)

9. J.Argyris, L.Tenek, "A practicable and locking-free laminated shallow shell triangular element of varying and adaptable curvature" *Computer Methods Appl.Mech.Engrg.*, 119, 215-82 (1994)

10. F.Keulen, J.Booij, "Refined consistent formulation of a curved triangular finite rotation shell element", *Inter.J.Numer.Methods Engrg.*, **39**, 2803-2820 (1996)

11. S.Ahmad, B.M.Irons, O.C.Zienkiewicz, "Analysis of thick and thin shell structures by curved finite elements", *Inter.J.Numer.Methods Engrg*., **42**, 419-451 (1970)

12. K.Y.Sze, "An explicit hybrid-stabilized 9-node Lagrangian shell element", *Computer Methods Appl.Mech.Engrg.*, **117**, 361-379 (1994)

13. K.Y.Sze, Y.S.Sim, A.K.Soh, "A hybrid stress quadrilateral shell element with full rotational d.o.f.s" *Inter.J.Numerical Methods Engrg*., **40**, 1785-1800 (1997)

14. Y.C.Fung, *Foundation of Solid Mechanics*, Prentice-Hall, Englewood Cliffs, New Jersey, 1965

15. T.J.R.Hughes, *The Finite Element Method - linear static and dynamic finite element analysis*, Prentice-Hall, New Jersey, 1987

16. K.Y.Sze, C.L.Chow, W.-J.Chen, “On invariance of isoparametric hybrid elements”, *Commun.Numerical Methods Engrg.*, **8**, 385-406 (1992)

17. R.H.MacNeal, R.L.Harder, “A proposed standard set of problems to test finite element accuracy”, *Finite Elements in Analysis & Design*, **1**, 3-20 (1985)

18. S.P.Timoshenko, S.Woinowsky-Krieger, *Theory of Plates and Shells*, McGraw-Hill, New York, 1970

19. T.Belytschko, B.K.Wong, "Assumed strain stabilization procedure for the 9-node Lagrange shell element", *Inter.J.Numer.Methods.Engrg.*, **28**, 385-414 (1989)

20. R.H.MacNeal, *Finite Elements : Their Design and Performance*, Marcel Dekker, New York, 1994

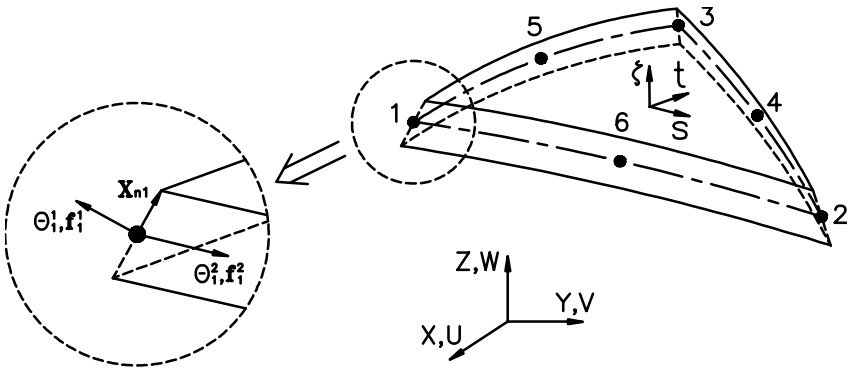


Fig.1. Description of a six-node degenerated shell element

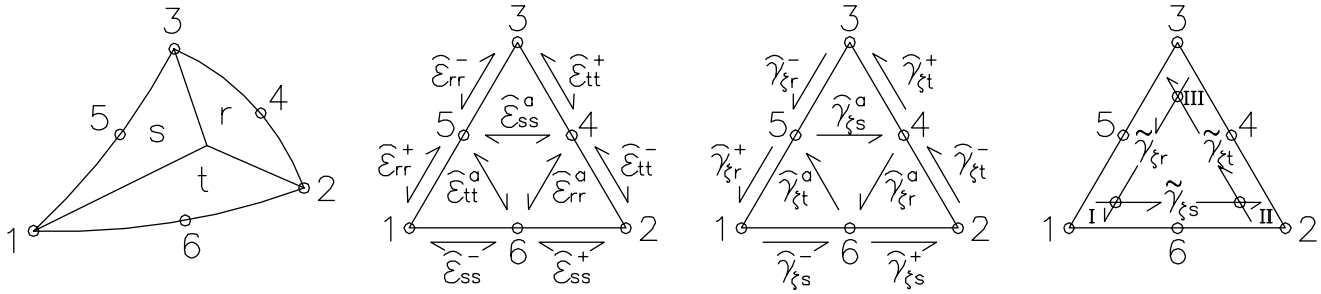


Fig.2. (a) The three area coordinates of the six-node element. (b) The employed natural membane and
bending natural strains. (c) The employed natural shear strains. (d) The employed interpolated natural shear strain components at the three integration stations

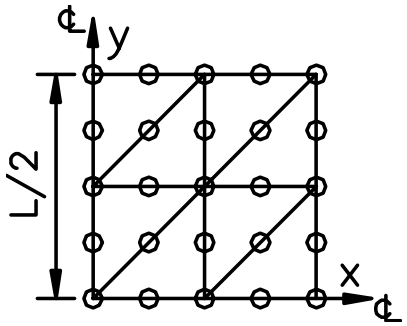


Fig.3. A quadrant of a plate modelled by 8 elements, Poisson's ratio equal to 0.3

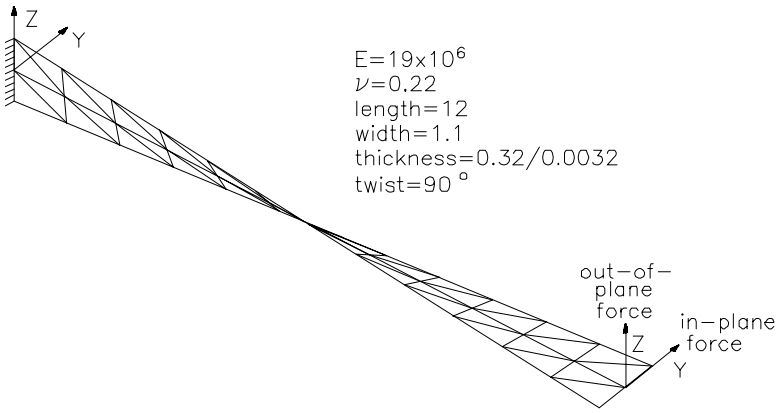


Fig.4. Twisted beam problem modelled by 5×25 nodes/side

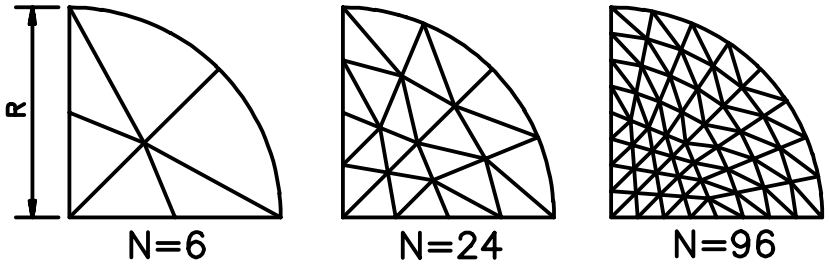


Fig.5. Meshes for circular plate (N is the number of elements), Poisson's ratio equal to 0.3

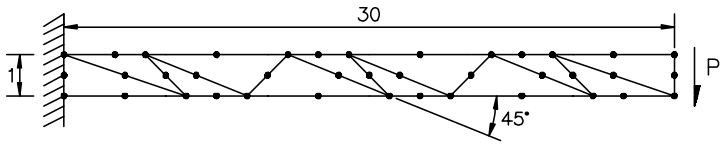


(a) overview of the cantilever

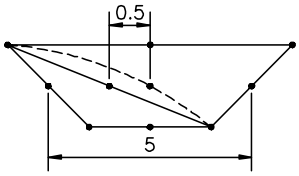


(b) detail of modelling schemes

Fig.6. A cantilever beam of unit thickness subjected to end shear, Poisson's ratio equal to 0.3

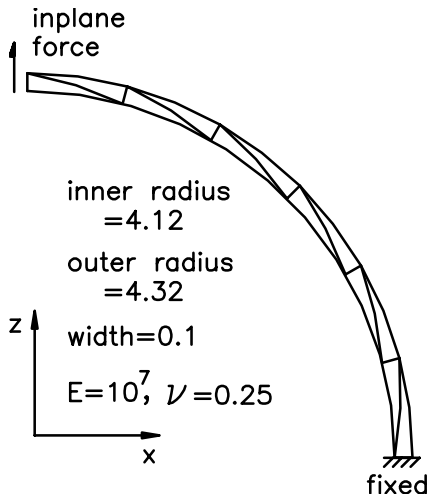


Fig.7. MacNeal & Harder's curved beam problem

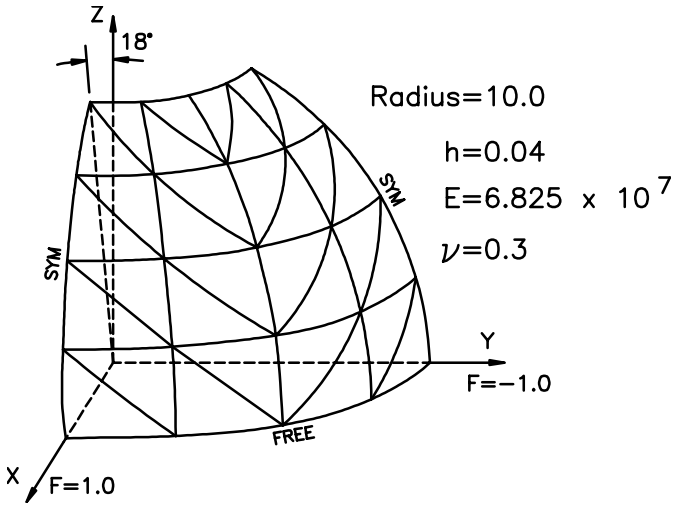


Fig.8. Hemispherical shell modelled by 9 nodes/side

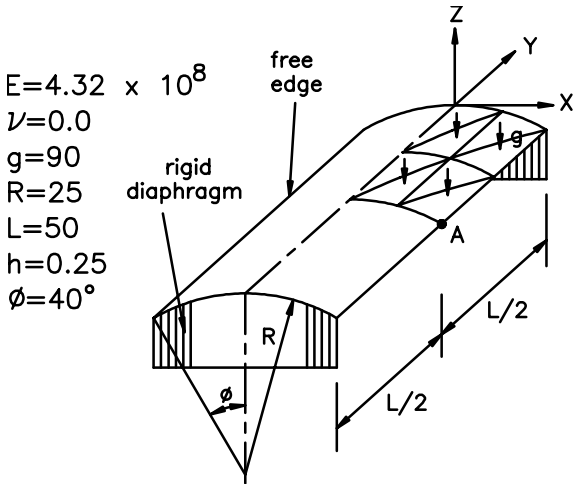


Fig.9. Scordelis-Lo roof modelled by 5 nodes/side

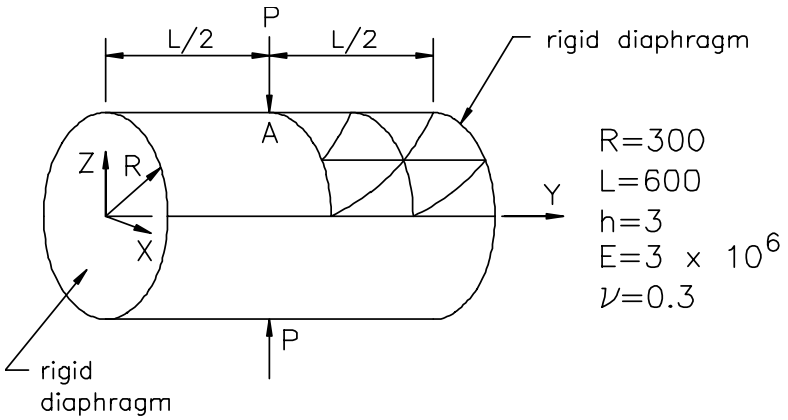


Fig.10. Pinched cylindrical shell modelled 5 nodes/side